CRYSTAL GROWTH & DESIGN

pubs.acs.org/crystal

Article

Solid-State ^{1}H, ^{13}C, and ^{17}O NMR Characterization of the Two Uncommon Polymorphs of Curcumin

Yizhe Dai, Victor Terskikh, Andreas Brinmkmann, and Gang Wu*

Cite This: *Cryst. Growth Des.* 2020, 20, 7484–7491

Read Online

ACCESS | Metrics & More | Article Recommendations | Supporting Information

ABSTRACT: Curcumin is known to exist in three polymorphs (forms I, II, and III) in the solid state. The most common polymorph of curcumin (form I) is monoclinic in the space group $P2/n$, whereas the other two uncommon forms are both orthorhombic with the space groups of $Pca2_1$ and $Pbca$ for forms II and III, respectively. While crystal structures are known for all three polymorphs of curcumin, their solid-state NMR signatures are incomplete in the literature. In this study, we report a complete set of solid-state ^{1}H, ^{13}C, and ^{17}O NMR data for form III of curcumin. In addition, we discovered that form III of curcumin prepared by repeated drying from methanol is not stable, which undergoes slow structural transition to form II in the solid state over a period of days at room temperature. As a result, we were able to obtain new solid-state ^{17}O NMR data for form II of curcumin, which complements the existing solid-state ^{1}H and ^{13}C NMR data for this polymorph in the literature. We compare experimental NMR parameters with calculated values by the GIPAW DFT and dispersion corrected DFT-D2 methods. We found that while the computed ^{13}C chemical shifts are generally in excellent agreement with experimental values, the quality of the computed ^{1}H and ^{17}O NMR chemical shifts is less satisfactory. This may imply that it is necessary to include the nuclear quantum effects in future quantum chemical calculations to account for potential proton tunneling and dynamics.

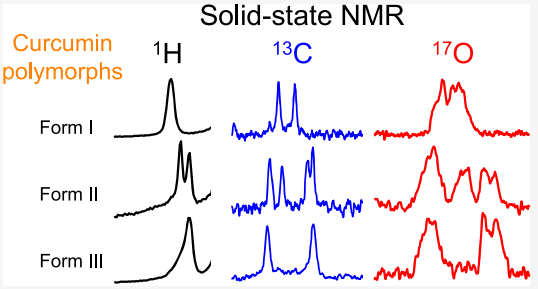

1. INTRODUCTION

Curcumin is a key component of turmeric that is produced by the plant *Curcuma longa* of the ginger family (*Zingiberaceae*). The biological activities of curcumin and related curcuminoids have been the focus of intense studies in recent years.[1−10] Although curcumin is commonly referred to by the chemical name of (1*E*,6*E*)-1,7-bis(4-hydroxy-3-methoxyphenyl)-1,6-heptadiene-3,5-dione (belonging to a general class of organic compounds known as 1,3-diketones or β-diketones), it exits in the solid state exclusively as the keto−enol tautomer, as illustrated in Scheme 1. Thus, the proper chemical name for curcumin should be (1*E*,4*Z*,6*E*)-5-hydroxy-1,7-bis(4-hydroxy-3-methoxyphenyl)-hepta-1,4,6-trien-3-one. Like many natural products, curcumin is known to exhibit polymorphism in the solid state. The polymorphism of curcumin has also been explored to improve its bioavailability with better drug formulation.[11−14] The first crystal structure of curcumin was reported by Tonnesen et al. in 1982.[15] This monoclinic polymorph with the space group $P2/n$ ($Z = 4$; $Z' = 1$) is the most common one, often denoted as form I. Several subsequent studies of curcumin further confirmed the crystal structure of form I.[16−18] In 2011, Sanphui et al.[17] discovered two new polymorphs of curcumin: forms II and III. Both of the new polymorphs are orthorhombic with the space groups of $Pca2_1$ ($Z = 8$; $Z' = 2$) and $Pbca$ ($Z = 8$; $Z' = 1$) for forms II and III, respectively. The overall molecular structures and crystal packing are quite similar in forms II and III. The most

Scheme 1. (Upper) Resonance Structures Including the Resonance-Assisted Hydrogen Bonding (RAHB) Model for Keto−Enol Tautomers of 1,3-Diketones. (Lower) Molecular Structure of Curcumin

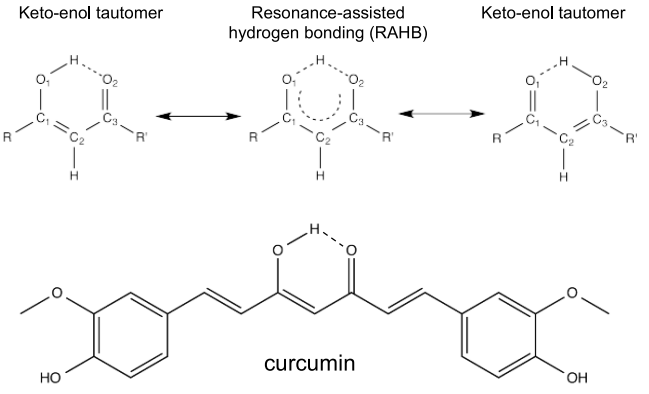

Received: August 19, 2020
Revised: October 6, 2020
Published: October 14, 2020

important structural difference between forms II and III is that form II has two independent curcumin molecules in the asymmetric unit cell, whereas form III has only one. Although Sanphui et al.[17] also reported solid-state ^{13}C NMR spectra for all three polymorphs of curcumin, their samples of forms II and III used in the solid-state NMR experiments were later proven to contain impurities, as recently pointed out by Wasylishen and co-workers.[19] The most complete solid-state NMR characterization of curcumin in form I was reported by Kong et al.[20] in 2016, which included solid-state ^{1}H, ^{2}H, ^{13}C, and ^{17}O NMR data, together with periodic DFT results obtained with the GIPAW method. In 2018, Wasylishen and co-workers[19] reported correct solid-state ^{1}H and ^{13}C NMR spectra for form II curcumin. However, the question regarding the solid-state ^{13}C NMR data reported by Sanphui et al.[17] for form III curcumin is still unresolved. In addition, form III of curcumin was known to be metastable. As a result, there is no standard solid-state ^{13}C NMR data reported for form III of curcumin in the literature. While other techniques such as powder X-ray diffraction (PXRD) and scanning electron microscopy (SEM) are also commonly used in studies of polymorphism of curcumin,[17,21,22] solid-state NMR appears to be the most effective in offering the clearest interpretation.

Solid-state NMR is a powerful tool for studying polymorphism of organic molecular solids, especially pharmaceuticals.[23−31] Most solid-state NMR studies of pharmaceutical molecules have employed ^{1}H and ^{13}C as NMR probes because of the ease in obtaining NMR signals from these nuclei at their natural abundance levels. However, recent studies have shown that, with isotopic ^{17}O-labeling, it is possible to obtain solid-state ^{17}O NMR spectra for organic and biological molecules and use them to complement the ^{1}H and ^{13}C NMR data for these molecules.[32−35] In principle, one should be able to obtain more complete information about molecular structure and bonding by studying all magnetic nuclei available in a molecule such as ^{1}H, ^{13}C, and ^{17}O. A few recent examples demonstrated the utility of this approach in studying a variety of chemical compounds including pharmaceutical compounds.[36−41] In this work, we report new solid-state ^{1}H, ^{13}C, and ^{17}O NMR data for forms II and III of curcumin. In particular, we obtained a complete set of solid-state ^{1}H, ^{13}C, and ^{17}O NMR data for form III and new solid-state ^{17}O NMR data for form II. These new results, together with those available in the literature for forms I and II, constitute a complete set of solid-state NMR signatures for all known polymorphs of curcumin.

2. EXPERIMENTAL SECTION

Curcumin was purchased from Alfa Aesar (95% purity). ^{17}O-Labeled curcumin was prepared by following the method reported by Kong et al.[20] In particular, the commercial curcumin was first recrystallized twice from methanol to remove minor impurities. The purified curcumin (200 mg) was dissolved in 17 mL MeOH (0.1% H_2O content), followed by addition of ^{17}O-enriched water (200 mg, 40% ^{17}O, purchased from CortecNet) and prewashed Amberlite IR-120 ion-exchange resin (100 mg strongly acidic form). The mixture was kept at 65 °C (oil bath) for 3 h. After the resin was removed, the mixture was concentrated to a small volume. The resulting solids were collected, washed with cold water (4 mL) and ether (3 × 1 mL), and dried under vacuum (yield 165 mg). The ^{17}O-enrichment level in the ^{17}O-labeled curcumin was determined to be 20% by comparing the ^{17}O NMR signal of the compound with that of the solvent (acetone) in a solution ^{17}O NMR spectrum. Form I of curcumin was prepared from recrystallization from MeOH. Form III was obtained in the following manner. Form I of curcumin was dissolved in MeOH and dried quickly with a stream of $N_2(g)$. This process was repeated several times. Initially, the solid was a mixture of 80% form I and 20% form III. After several cycles, the compound became pure form III as monitored by solid-state ^{1}H NMR (see Figure S1 in the Supporting Information). In some cases, a trace amount of form I (<5%) remained. However, we found that the form III samples prepared in the above fashion were not stable and underwent solid-state transformation to form II in days at room temperature. Thus, this turned out to be another way of preparing form II, which was known to be difficult to prepare in a reliable fashion.[19] More stable form III crystals were made by recrystallization of the unstable form III solids from MeOH with seeding. The resultant crystals of form III were stable on the bench for months (see Figure S2 in the Supporting Information).

Solid-state ^{1}H, ^{13}C, and ^{17}O NMR experiments were performed on a Bruker NEO-700 (16.4 T) spectrometer with a Bruker 2.5 mm MAS probe. In the ^{13}C CP/MAS experiments, a contact time of 2 ms was used and the ^{1}H decoupling field was about 100 kHz. A rotor-synchronized Hahn-echo sequence was used for recording both ^{1}H and ^{17}O MAS NMR spectra to eliminate the acoustic ringing and the background signal from the probe. For the ^{17}O MAS experiments, no proton decoupling was applied. The 90° pulse width for the ^{17}O central transition was 1.0 μs. The recycle delays used in different solid-state NMR experiments were as follows: 60 s for ^{1}H; 10 s for ^{13}C; 5 s for ^{17}O. Sample temperatures under MAS conditions were calibrated with the ^{79}Br NMR signal from a solid KBr sample.[42] All ^{13}C chemical shifts were referenced to the signal of 1% TMS in $CDCl_3$ (δ = 0 ppm) by setting the ^{13}C NMR signal of the carboxylate group of solid α-glycine to 176.5 ppm.[43] All ^{1}H and ^{17}O chemical shifts were referenced to 1% TMS in $CDCl_3$ and neat D_2O(liq), respectively, by using the frequency ratio (Ξ) values from the literature (for ^{1}H, Ξ = 100.000000%; for ^{13}C, Ξ = 25.145020%; for ^{17}O, Ξ = 13.556457%)[44] and the ^{13}C frequency for 1% TMS in $CDCl_3$. Spectral simulations were performed with DMfit.[45]

All quantum chemical calculations were performed using the Cambridge Sequential Total Energy Package (CASTEP) code[46] (ver. 2017) implemented within BIOVIA's Materials Studio. CASTEP employs DFT using the plane-wave pseudopotential approach. The generalized gradient approximation with the Perdew−Burke−Ernzerhof exchange correlation functional[47] was chosen. First, geometry optimization was performed employing the Broyden−Fletcher−Goldfarb−Shanno (BFGS) algorithm together with OTFG on-the-fly ultrasoft pseudopotentials (version 2017R2), a cutoff energy of 571.4 eV and a 1 × 2 × 1 k-point grid. Subsequently, the NMR parameters were calculated using the gauge including the projector augmented waves (GIPAW) method implemented in the NMR module of CASTEP,[48,49] employing OTFG on-the-fly pseudopotentials (version 00), a cutoff energy of 610 eV, and a 1 × 2 × 1 k-point grid. Calculated isotropic magnetic shielding values were converted to calculated isotropic chemical shift values as follows: for ^{1}H, δ/ppm (calc.) = 29.0/ppm − σ/ppm (calc.); for ^{13}C, δ/ppm (calc.) = 170.4/ppm − σ/ppm (calc.); for ^{17}O, δ/ppm (calc.) = 287.0/ppm − σ/ppm (calc.).

For the dispersion-corrected DFT calculations (DFT-D2), the geometry optimization step was performed using the revised Perdew−Burke−Ernzerhof exchange correlation functional,[50] OTFG on-the-fly ultrasoft pseudopotentials (version 2017R2), a cutoff energy of 571.4 eV, and a 1 × 2 × 1 k-point grid. Dispersion was included through the reparameterization of the two-body force field developed by Grimme (D2).[51] For the damping parameter d, values of 3.5[52] and 5.0[53] were used. Subsequently, the NMR parameters were calculated with the same computational settings as for the geometry optimization step except for omitting the dispersion correction. The following conversions were used between calculated isotropic magnetic shielding values and isotropic chemical shift values: for ^{1}H, δ/ppm (calc.) = 30.0/ppm − σ/ppm (calc.); for ^{13}C, δ/ppm (calc.) = 175.0/ppm − σ/ppm (calc.); for ^{17}O, δ/ppm (calc.) = 275/ppm − σ/ppm (calc.).

https://dx.doi.org/10.1021/acs.cgd.0c01164
Cryst. Growth Des. 2020, 20, 7484−7491

3. RESULTS AND DISCUSSION

Figure 1 shows the solid-state ^{1}H NMR spectra obtained under the MAS condition for the three polymorphs of curcumin. In

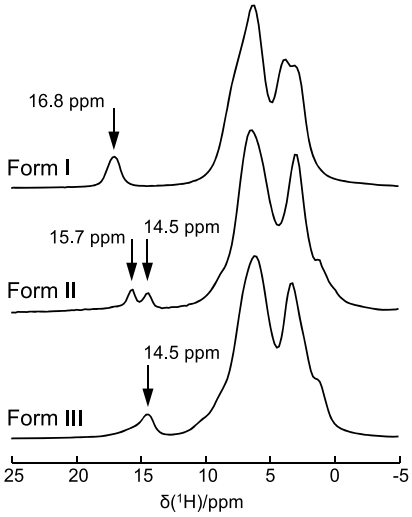

Figure 1. Experimental ^{1}H MAS NMR spectra of the three polymorphs of curcumin. All ^{1}H MAS spectra were recorded at 16.4 T (700 MHz for ^{1}H) with a sample spinning frequency of 30 kHz. The sample temperature was controlled at 293 K.

all cases, the ^{1}H NMR signals from the enolic protons are clearly resolved. The ^{1}H chemical shifts observed for forms I and II are in excellent agreement with the literature results.[19,20] For form III, the ^{1}H chemical shift of the enolic proton is 14.5 ppm. Interestingly, this value is similar to that found for molecule B in form II of curcumin. Further, in contrast to the situation seen in form II, only one enolic proton signal was observed for form III, which is consistent with the crystal structure of form III (only one molecule is in the asymmetric unit cell).[17]

Figure 2 shows the ^{13}C CP/MAS NMR spectra obtained for the three polymorphs of curcumin. For form I, the ^{13}C chemical shifts for C_1 and C_3 are found at 187.4 and 182.7 ppm, respectively. In contrast, a total of four signals were observed for form II in the same spectral region: 189.6, 186.2, 179.2, and 177.8 ppm. These results for forms I and II are in excellent agreement with what have been reported in the literature.[19,20] In addition, as Wasylishen and co-workers[19] recently showed, the ^{13}C NMR signals at 189.6 and 177.8 ppm for form II are due to molecule B, whereas the enolic proton displays a ^{1}H chemical shift of 14.5 ppm. For molecule A of form II, the ^{13}C NMR signals are found to be at 186.2 and 179.2 and the enolic proton at 15.7 ppm. For form III, we found that the ^{13}C NMR signals for C_1 and C_3 appear at 190.2 and 177.8 ppm, respectively, and the enolic proton at 14.5 ppm. Thus, it seems that the ^{1}H and ^{13}C NMR signals for form III resemble those observed for molecule B of form II. This general trend is also seen in the ^{17}O MAS NMR spectra obtained for the three polymorphs of curcumin, as shown in Figure 3. We should note that, while three resolved ^{17}O NMR signals are observed in the spectrum of form II, the signal at the high-frequency end exhibits higher intensity suggesting the presence of two overlapping signals. Indeed, we were able to extract the ^{17}O NMR parameters for the two overlapping sites by spectral simulation, as seen in Figure 3. We also obtained ^{17}O MAS NMR spectra of form II at a higher magnetic field, 21.1 T, and confirmed the ^{17}O NMR parameters for all four sites (see Figure S3 in the Supporting Information). Thus, the fact that a total of four ^{17}O NMR signals are observed for form II is in agreement with the observation in solid-state ^{13}C NMR mentioned earlier. We can then assign the four ^{17}O NMR signals in a similar way as done for the four ^{13}C NMR signals. As also seen in Figure 3, only two ^{17}O NMR signals are detected for form III, and their ^{17}O NMR parameters (chemical shifts and quadrupole parameters) are similar to those for molecule B of form II. Further, the enolic proton in form III has a ^{1}H chemical shift of 14.5 ppm, which is identical to that seen for molecule B of form II. All experimental ^{1}H, ^{13}C, and ^{17}O NMR parameters are summarized in Table 1.

Among the three polymorphs of curcumin, there are four crystallographically distinct curcumin molecules. Now that we

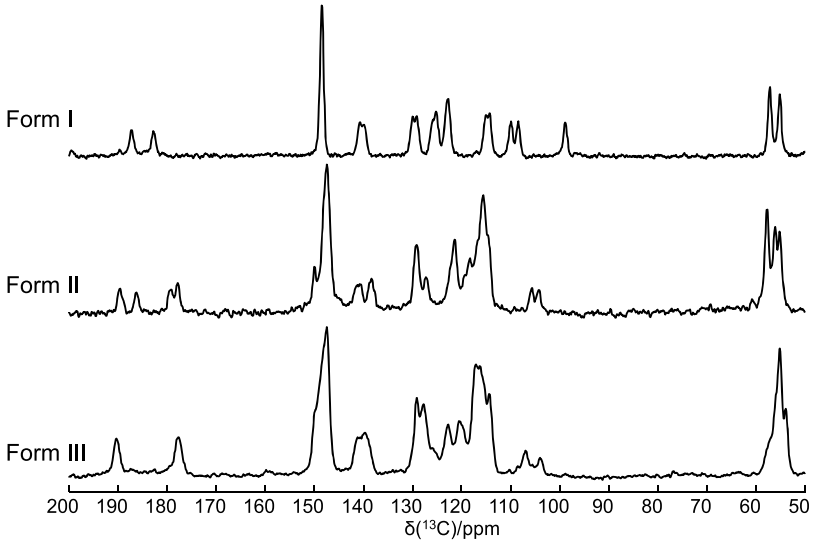

Figure 2. Experimental ^{13}C CP/MAS NMR spectra of the three polymorphs of curcumin. All spectra were recorded at 16.4 T (700 MHz for ^{1}H and 176 MHz for ^{13}C) with a sample spinning frequency of 20 kHz. The sample temperature was controlled at 293 K. Note that a trace amount of form I (<5%) was present in the sample of form III.

https://dx.doi.org/10.1021/acs.cgd.0c01164
Cryst. Growth Des. 2020, 20, 7484−7491

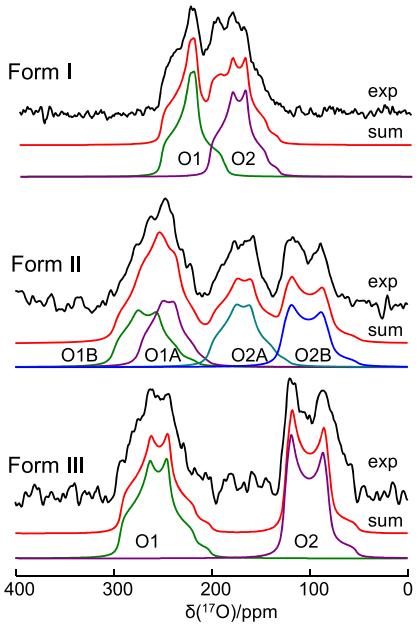

Figure 3. Experimental (black traces) and simulated (colored traces) ^{17}O MAS NMR spectra of the three polymorphs of curcumin. All spectra were recorded at 16.4 T (700 MHz for ^{1}H and 94 MHz for ^{17}O) with a sample spinning frequency of 30 kHz. The sample temperature was controlled at 293 K.

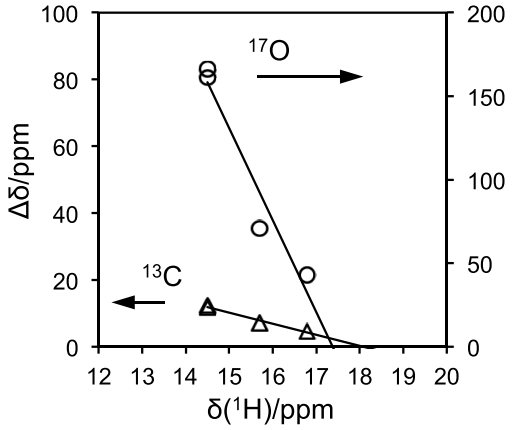

Figure 4. Correlation between chemical shift difference (^{13}C and ^{17}O) and the ^{1}H chemical shift for the enolic proton in three polymorphs of curcumin. The chemical shift difference is defined as $\Delta\delta(^{13}C) = \delta(^{13}C_1) - \delta(^{13}C_3)$ and $\Delta\delta(^{17}O) = \delta(^{17}O_1) - \delta(^{17}O_2)$.

have obtained a complete set of ^{1}H, ^{13}C, and ^{17}O NMR data for all four molecules provides an excellent opportunity to look into the relationship between NMR parameters (^{13}C and ^{17}O chemical shifts and ^{17}O quadrupole couplings) and molecular structure. We found that in each case the curcumin molecule is nonsymmetric. That is, the C_1-O_1 and C_3-O_2 halves of the molecule are different, resulting in two sets of NMR signals for each curcumin molecule. Interestingly, after examining the NMR data presented in Table 1, we found that the ^{13}C and ^{17}O chemical shift differences between the C_1-O_1 and C_3-O_2 halves of the molecule (i.e., $\Delta\delta(^{13}C) = \delta(^{13}C_1) - \delta(^{13}C_3)$ and $\Delta\delta(^{17}O) = \delta(^{17}O_1) - \delta(^{17}O_2)$) are clearly correlated with the ^{1}H chemical shift of the central enolic proton. As illustrated in Figure 4, the chemical shift difference appears to decrease with the increase in $\delta(^{1}H)$ of the enolic proton. Furthermore, two general trends in Figure 4 are worth noting. First, the slope of the ^{17}O line is about 10 times steeper than that of the ^{13}C line. This reflects the remarkable sensitivity of ^{17}O NMR parameters on molecular structure and chemical bonding. Second, the ^{13}C and ^{17}O data points converge to a narrow ^{1}H chemical shift range between 17.5 and 18.0 ppm. This means that, if a curcumin molecule displays a symmetric $O_1\cdots H\cdots O_2$ hydrogen bond as fully depicted by the RAHB model[54] shown in Scheme 1, the ^{1}H chemical shift for the enolic proton would be about 17.5−18.0 ppm. Thus, the plots shown in Figure 4 suggest that the $O_1\cdots H\cdots O_2$ hydrogen bond in form I is the least asymmetric among the three forms of curcumin. However, we caution that such an interpretation should be restricted to different polymorphs of the same molecule. For example, Kong et al.[20] reported the following NMR parameters for the $O_1\cdots H\cdots O_2$ hydrogen bond in dibenzoylmethane: $\delta(^{1}H) = 17.5$ ppm, $\Delta\delta(^{13}C) = \delta(^{13}C_1) - \delta(^{13}C_3) = 5.3$ ppm, and $\Delta\delta(^{17}O) = \delta(^{17}O_1) - \delta(^{17}O_2) = 72$ ppm. These data points clearly lie outside the two straight lines shown in Figure 4.

Now we can also examine structural variations among the four curcumin molecules on the basis of their crystal structures.

Table 1. Summary of Experimental and GIPAW Computed Solid-State ^{1}H, ^{13}C, and ^{17}O NMR Parameters for Selected Atoms around the 1,3-Enol Moiety (shown below) in Three Polymorphs of Curcumin[a]

	δ_{iso}/ppm						C_Q/MHz		η_Q	
Polymorph	H1	C3	C2	C1	O1	O2	O1	O2	O1	O2
Form I[b]										
Exptl.	16.8	182.7	99.0	187.4	252	209	−6.2	−6.0	0.90	0.60
Compt.	16.0	181.2	103.2	187.3	272	183	−6.9	−7.2	0.91	0.23
Form II[c]										
Exptl. (A)	15.7	179.1	105.7	186.2	276	197	6.2	−6.8	0.60	0.60
Exptl. (B)	14.5	177.8	104.3	189.6	295	133	7.1	−7.1	0.50	0.20
Compt. (A)	14.2	178.6	112.3	185.6	278	156	7.0	−7.4	0.95	0.28
Compt. (B)	16.2	177.3	110.5	188.8	332	153	7.4	−7.2	0.62	0.16
Form III[d]										
Exptl.	14.5	177.8	106.9	190.2	295	134	−6.9	−7.0	0.70	0.15
Comput.	15.5	177.7	110.7	186.0	291	160	−6.8	−7.3	0.99	0.21

[a]Uncertainties in experimental results are estimated to be $\delta_{iso}(^{1}H)$, ±0.1 ppm; $\delta_{iso}(^{13}C)$, ±0.1 ppm; $\delta_{iso}(^{17}O)$, ±2 ppm; $C_Q(^{17}O)$, ±0.5 MHz; $\eta_Q(^{17}O)$, ±0.2. The sign of the experimental $C_Q(^{17}O)$ was assumed to be the same as that of the computed one. [b]From ref 20. [c]From ref 19, except for the ^{17}O NMR data which are from this work. [d]This work.

https://dx.doi.org/10.1021/acs.cgd.0c01164
Cryst. Growth Des. 2020, 20, 7484−7491

The key bond distances in the keto−enol core of the curcumin molecule are shown in Figure 5. In general, for hydrogen

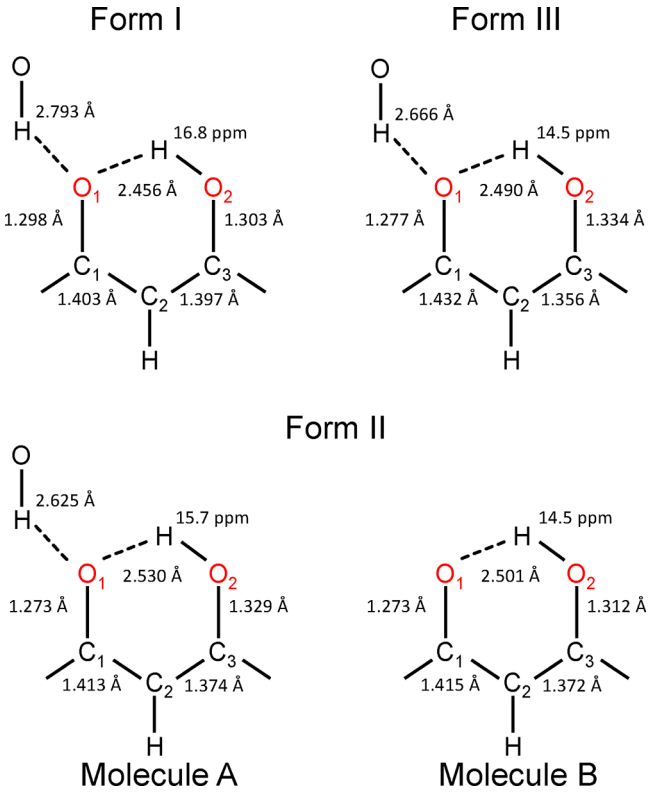

Figure 5. Selected bond distances and an additional hydrogen bond around the keto−enol core of each curcumin molecule found in the three polymorphs of curcumin. The ^{1}H chemical shifts are also shown.

bonds of the O−H···O type, the ^{1}H chemical shift is expected to be correlated with $r_{O\cdots O}$.[55−59] However, as seen from Figure 5, this is not the case among the four curcumin molecules, suggesting that other factors are in play in these cases. Indeed, as noted by previous workers,[17,19] three of the four curcumin molecules experience additional hydrogen bonding around the central keto−enol core of the molecule, as also highlighted in Figure 5. In particular, for the curcumin molecules in forms I and III as well as molecule A in form II, O_1 forms a hydrogen bond with the phenolic OH group from a neighboring molecule. We speculate that this additional hydrogen bond may play an important role in influencing the ^{1}H chemical shift for the enolic proton. We also attempted to link the observed ^{13}C and ^{17}O chemical shifts to the structural features. The key measure is the difference between the C_1-O_1 and C_3-O_2 bond lengths. The smaller this difference, the more similar the ^{13}C or ^{17}O chemical shifts observed for the two halves of the molecule. For example, in form III, this bond-length difference is 1.334−1.277 = 0.057 Å, whereas the corresponding value for the curcumin molecule in form I is only 0.007 Å. Thus, the curcumin molecule in form III can be described, to a greater degree, by the $C_1{=}O_1$ and C_3-O_2-H bonding schemes, which results in a greater difference between the two sets of ^{13}C or ^{17}O NMR signals. We should note that this argument cannot explain the trends seen for molecules A and B in form II. Once again, a key difference between molecules A and B in form II is the presence of an additional hydrogen bond only in molecule A.

In two previous studies of curcumin,[19,20] experimental ^{1}H, ^{13}C, and ^{17}O NMR results for forms I and II were compared with computational data. Here, we are able to examine the accuracy of computational results for all three polymorphs. Table 1 also shows the computed results based on the GIPAW DFT method. As shown in Figure 6, the computed chemical

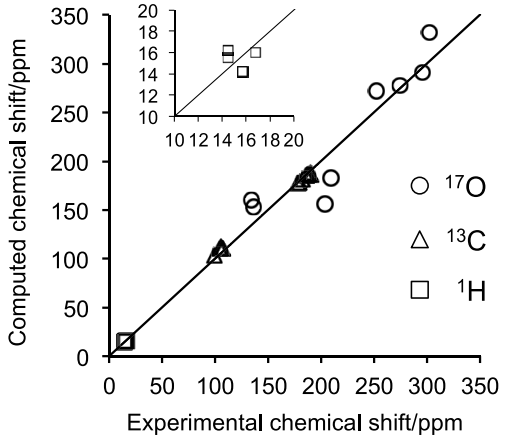

Figure 6. Comparison between experimental and computed ^{1}H, ^{13}C, and ^{17}O chemical shifts for the three polymorphs of curcumin. The diagonal line is shown to aid in visual inspection of data. The inset shows the expanded region around the ^{1}H chemical shift data points.

shifts are generally consistent with the experimental values. However, it is important to point out that, while the experimental ^{13}C chemical shifts are very well reproduced by the GIPAW DFT computation, the agreements between experimental and computed for ^{1}H and ^{17}O chemical shifts are considerably poorer. For example, as noted by Wasylishen and co-workers[19] in their recent study, the GIPAW DFT calculation was unable to reproduce the trend in the ^{1}H chemical shifts observed for form II; see the inset of Figure 6. This particular difficulty in computing ^{1}H and ^{17}O chemical shifts around the keto−enol moiety of the molecule may be related to the type of hydrogen bonding interaction that these atoms are involved in. Curcumin, together with many 1,3-diketone molecules, is a well-known example where the O−H···O hydrogen bond in its keto−enol tautomer can be considered to be a low-barrier hydrogen bond (LBHB).[60−71] As pointed out by many previous workers, it is more instructive to view the proton involved in a LBHB as a nuclear wave function rather than to ask about its precise "location or position". It is not difficult to see why the ^{1}H and ^{17}O chemical shifts should be more sensitive to such nuclear quantum effects. Similar trends were seen in the calculated ^{17}O quadrupole parameters. As seen in Table 1, although the ^{17}O quadrupole coupling constants are reasonably reproduced by the GIPAW DFT calculations, the asymmetry parameters display considerable discrepancies. It is also noted that the largest discrepancies are found for form I and for molecule A of form II. Indeed, these two cases have the greatest LBHB characters.

To further examine the origin of the poor calculated ^{1}H and ^{17}O chemical shifts, we carried out additional dispersion-corrected DFT-D2 calculations for all three polymorphs of curcumin. We found that, while the ^{13}C chemical shifts change

https://dx.doi.org/10.1021/acs.cgd.0c01164
Cryst. Growth Des. 2020, 20, 7484−7491

very little as compared with those from regular GIPAW DFT calculations, the ^{1}H and ^{17}O chemical shifts showed even worse agreement with the experimental data; see Figure S4 in the Supporting Information. The most pronounced changes occurred for form I. A close inspection of the molecular geometries reveals that the dispersion-corrected DFT-D2 method tends to make the $O_1\cdots H\cdots O_2$ LBHB in form I curcumin more like a regular $O_1\cdots H-O_2$ HB. That is, the enolic proton was moved closer to the O_2 atom resulting two very different C_1-O_1 and C_3-O_2 bond distances. As seen from Figure 5, form I has the greatest character of a LBHB among the three polymorphs (i.e., the difference between the C_1-O_1 and C_3-O_2 bond lengths is the smallest). Thus, we can conclude that, while the dispersion corrected DFT-D2 can improve the accuracy of computed chemical shifts in molecular systems containing regular HBs, this is not the case for LBHBs. This observation is not totally unexpected, because the dispersion forces that are included in DFT-D2 are fundamentally different from the nuclear quantum effects. Perhaps calculations based on path-integral molecular dynamics (PIMD)[72] are better suited to treat the nuclear quantum effects seen in curcumin.

4. CONCLUSIONS

We have reported solid-state ^{1}H, ^{13}C, and ^{17}O NMR characterization for the two uncommon polymorphs of curcumin, known as forms II and III. This is the first time that complete solid-state ^{1}H, ^{13}C, and ^{17}O NMR signatures are available for all three polymorphs of curcumin. These data can serve as standards in future solid-state NMR studies of curcumin polymorphism. The new solid-state ^{17}O NMR data appear to exhibit a parallelism with the ^{13}C NMR data, but display greater sensitivity toward changes in molecular structure and chemical bonding. We have also supplemented solid-state NMR experiments with GIPAW DFT calculations. While the GIPAW DFT computation produces excellent ^{13}C chemical shifts, the agreement between experimental and computational results is less satisfactory for ^{1}H and ^{17}O chemical shifts. Further, we showed that the computed ^{1}H and ^{17}O chemical shifts in curcumin were not improved by the dispersion corrected DFT-D2 method. This observation suggests that it is important to explicitly consider nuclear quantum effects in systems where LBHBs are present. In this respect, curcumin may be used as a good test case in any future computational study.

■ ASSOCIATED CONTENT

Supporting Information

The Supporting Information is available free of charge at https://pubs.acs.org/doi/10.1021/acs.cgd.0c01164.

^{1}H MAS NMR spectra showing the conversion from form I to form III. Stability of form III crystals monitored by ^{13}C CP/MAS NMR. ^{17}O MAS spectrum of form III obtained at 21.1 T. Computational results from DFT-D2. A complete list of computed ^{1}H and ^{13}C chemical shifts. (PDF)

■ AUTHOR INFORMATION

Corresponding Author

Gang Wu − *Department of Chemistry, Queen's University, Kingston, Ontario K7L 3N6, Canada;* orcid.org/0000-0002-0936-9432; Email: wugang@queensu.ca

Authors

Yizhe Dai − *Department of Chemistry, Queen's University, Kingston, Ontario K7L 3N6, Canada*

Victor Terskikh − *Department of Chemistry, Queen's University, Kingston, Ontario K7L 3N6, Canada; Metrology, National Research Council Canada, Ottawa, Ontario K1A 0R6, Canada;* orcid.org/0000-0003-1514-2610

Andreas Brinmkmann − *Metrology, National Research Council Canada, Ottawa, Ontario K1A 0R6, Canada;* orcid.org/0000-0001-6442-3780

Complete contact information is available at: https://pubs.acs.org/10.1021/acs.cgd.0c01164

Notes

The authors declare no competing financial interest.

■ ACKNOWLEDGMENTS

This work was supported by the Natural Sciences and Engineering Research Council (NSERC) of Canada. Access to the 900 MHz NMR spectrometer was provided by the National Ultrahigh Field NMR Facility for Solids (Ottawa, Canada), a national research facility funded by a consortium of Canadian universities, National Research Council Canada and Bruker BioSpin and managed by the University of Ottawa (http://nmr900.ca).

■ REFERENCES

(1) Goel, A.; Kunnumakkara, A. B.; Aggarwal, B. B. Curcumin as "Curecumin": From kitchen to clinic. *Biochem. Pharmacol.* **2008**, *75*, 787−809.

(2) Aggarwal, B. B.; Harikumar, K. B. Potential therapeutic effects of curcumin, the anti-inflammatory agent, against neurodegenerative, cardiovascular, pulmonary, metabolic, autoimmune and neoplastic diseases. *Int. J. Biochem. Cell Biol.* **2009**, *41*, 40−59.

(3) Esatbeyoglu, T.; Huebbe, P.; Ernst, I. M. A.; Chin, D.; Wagner, A. E.; Rimbach, G. Curcumin - From molecule to biological function. *Angew. Chem., Int. Ed.* **2012**, *51*, 5308−5332.

(4) Sinha, D.; Biswas, J.; Sung, B.; Aggarwal, B. B.; Bishayee, A. Chemopreventive and chemotherapeutic potential of curcumin in breast cancer. *Curr. Drug Targets* **2012**, *13*, 1799−1819.

(5) Salem, M.; Rohani, S.; Gillies, E. R. Curcumin, a promising anti-cancer therapeutic: a review of its chemical properties, bioactivity and approaches to cancer cell delivery. *RSC Adv.* **2014**, *4*, 10815−10829.

(6) Ghosh, S.; Banerjee, S.; Sil, P. C. The beneficial role of curcumin on inflammation, diabetes and neurodegenerative disease: A recent update. *Food Chem. Toxicol.* **2015**, *83*, 111−124.

(7) Nelson, K. M.; Dahlin, J. L.; Bisson, J.; Graham, J.; Pauli, G. F.; Walters, M. A. The Essential Medicinal Chemistry of Curcumin. *J. Med. Chem.* **2017**, *60*, 1620−1637.

(8) Cooksey, C. J. Turmeric: old spice, new spice. *Biotech. Histochem.* **2017**, *92*, 309−314.

(9) Arablou, T.; Kolahdouz-Mohammadi, R. Curcumin and endometriosis: Review on potential roles and molecular mechanisms. *Biomed. Pharmacother.* **2018**, *97*, 91−97.

(10) Tsuda, T. Curcumin: An Effective or Deceptive Dietary Factor? Challenges for Functional Food Scientists. *J. Agric. Food Chem.* **2018**, *66*, 1059−1060.

(11) Liu, J.; Svard, M.; Hippen, P.; Rasmuson, A. C. Solubility and Crystal Nucleation in Organic Solvents of Two Polymorphs of Curcumin. *J. Pharm. Sci.* **2015**, *104*, 2183−2189.

(12) Suresh, K.; Nangia, A. Curcumin: pharmaceutical solids as a platform to improve solubility and bioavailability. *CrystEngComm* **2018**, *20*, 3277−3296.

(13) Poppler, A.-C.; Lubtow, M. M.; Schlauersbach, J.; Wiest, J.; Meinel, L.; Luxenhofer, R. Loading-dependent structural model of

polymeric micelles encapsulating curcumin by solid-state NMR spectroscopy. *Angew. Chem., Int. Ed.* **2019**, *58*, 18540−18546.
(14) Del Prado-Audelo, M. L.; Caballero-Florán, I. H.; Meza-Toledo, J. A.; Mendoza-Muñoz, N.; González-Torres, M.; Florán, B.; Cortés, H.; Leyva-Gómez, G. Formulations of Curcumin Nanoparticles for Brain Diseases. *Biomolecules* **2019**, *9*, 56.
(15) Tonnesen, H. H.; Karlsen, J.; Mostad, A. Structural studies of curcuminoids. I. The crystal structure of curcumin. *Acta Chem. Scand.* **1982**, *36*, 475−479.
(16) Parimita, S. P.; Ramshankar, Y. V.; Suresh, S.; Guru Row, T. N. Redetermination of curcumin: (1E,4Z,6E)-5-hydroxy-1,7-bis(4-hydroxy-3-methoxyphenyl)hepta-1,4,6-trien-3-one. *Acta Crystallogr., Sect. E: Struct. Rep. Online* **2007**, *63*, o860−o862.
(17) Sanphui, P.; Goud, N. R.; Khandavilli, U. B. R.; Bhanoth, S.; Nangia, A. New polymorphs of curcumin. *Chem. Commun.* **2011**, *47*, 5013−5015.
(18) Reid, J. W.; Kaduk, J. A.; Garimella, S. V.; Tse, J. S. Rietveld refinement using synchrotron powder diffraction data for curcumin, $C_{21}H_{20}O_6$, and comparison with density functional theory. *Powder Diffr.* **2015**, *30*, 67−75.
(19) Matlinska, M.; Wasylishen, R. E.; Bernard, G. M.; Terskikh, V. V.; Brinkmann, A.; Michaelis, V. K. Capturing elusive polymorphs of Curcumin: A structural characterization and computational study. *Cryst. Growth Des.* **2018**, *18*, 5556−5563.
(20) Kong, X.; Brinkmann, A.; Terskikh, V.; Wasylishen, R. E.; Bernard, G. M.; Duan, Z.; Wu, Q.; Wu, G. Proton Probability Distribution in the O···H···O Low-Barrier Hydrogen Bond: A Combined Solid-State NMR and Quantum Chemical Computational Study of Dibenzoylmethane and Curcumin. *J. Phys. Chem. B* **2016**, *120*, 11692−11704.
(21) Thorat, A. A.; Dalvi, S. V. Particle formation pathways and polymorphism of curcumin induced by ultrasound and additives during liquid antisolvent precipitation. *CrystEngComm* **2014**, *16*, 11102−11114.
(22) Thorat, A. A.; Dalvi, S. V. Solid-State Phase Transformations and Storage Stability of Curcumin Polymorphs. *Cryst. Growth Des.* **2015**, *15*, 1757−1770.
(23) Harris, R. K. NMR studies of organic polymorphs & solvates. *Analyst (Cambridge, U. K.)* **2006**, *131*, 351−373.
(24) Harris, R. K. Applications of solid-state NMR to pharmaceutical polymorphism and related matters. *J. Pharm. Pharmacol.* **2007**, *59*, 225−239.
(25) Geppi, M.; Mollica, G.; Borsacchi, S.; Veracini, C. A. Solid-State NMR Studies of Pharmaceutical Systems. *Appl. Spectrosc. Rev.* **2008**, *43*, 202−302.
(26) Potrzebowski, M. J. Crystallography and NMR: Applications to organic and pharmaceutical chemistry. *eMagRes.* **2008**, 890−903.
(27) Rossini, A. J.; Widdifield, C. M.; Zagdoun, A.; Lelli, M.; Schwarzwälder, M.; Copéret, C.; Lesage, A.; Emsley, L. Dynamic Nuclear Polarization Enhanced NMR Spectroscopy for Pharmaceutical Formulations. *J. Am. Chem. Soc.* **2014**, *136*, 2324−2334.
(28) Vogt, F. G. Characterization of pharmaceutical compounds by solid-state NMR. *eMagRes.* **2015**, *4*, 255−268.
(29) Bryce, D. L. NMR crystallography: structure and properties of materials from solid-state nuclear magnetic resonance observables. *IUCrJ* **2017**, *4*, 350−359.
(30) Zhao, L.; Hanrahan, M. P.; Chakravarty, P.; DiPasquale, A. G.; Sirois, L. E.; Nagapudi, K.; Lubach, J. W.; Rossini, A. J. Characterization of Pharmaceutical Cocrystals and Salts by Dynamic Nuclear Polarization-Enhanced Solid-State NMR Spectroscopy. *Cryst. Growth Des.* **2018**, *18*, 2588−2601.
(31) Hodgkinson, P. NMR crystallography of molecular organics. *Prog. Nucl. Magn. Reson. Spectrosc.* **2020**, *118*−*119*, 10−53.
(32) Wu, G. Solid-state ^{17}O NMR studies of organic and biological molecules. *Prog. Nucl. Magn. Reson. Spectrosc.* **2008**, *52*, 118−169.
(33) Wong, A.; Poli, F. Solid-state ^{17}O NMR studies of biomolecules. *Annu. Rep. NMR Spectrosc.* **2014**, *83*, 145−220.
(34) Wu, G. Solid-State ^{17}O NMR studies of organic and biological molecules: Recent advances and future directions. *Solid State Nucl. Magn. Reson.* **2016**, *73*, 1−14.
(35) Wu, G. ^{17}O NMR studies of organic and biological molecules in aqueous solution and in the solid state. *Prog. Nucl. Magn. Reson. Spectrosc.* **2019**, *114*−*115*, 135−191.
(36) Hamaed, H.; Pawlowski, J. M.; Cooper, B. F. T.; Fu, R.; Eichhorn, S. H.; Schurko, R. W. Application of Solid-State ^{35}Cl NMR to the Structural Characterization of Hydrochloride Pharmaceuticals and their Polymorphs. *J. Am. Chem. Soc.* **2008**, *130*, 11056−11065.
(37) Wong, A.; Smith, M. E.; Terskikh, V.; Wu, G. Obtaining accurate chemical shifts for all magnetic nuclei (^{1}H, ^{13}C, ^{17}O, and ^{27}Al) in tris(2,4-pentanedionato-O, O')aluminium(III) — A solid-state NMR case study. *Can. J. Chem.* **2011**, *89*, 1087−1094.
(38) Wong, A.; Howes, A. P.; Yates, J. R.; Watts, A.; Anupold, T.; Past, J.; Samoson, A.; Dupree, R.; Smith, M. E. Ultra-high resolution ^{17}O solid-state NMR spectroscopy of biomolecules: A comprehensive spectral analysis of monosodium L-glutamate monohydrate. *Phys. Chem. Chem. Phys.* **2011**, *13*, 12213−12224.
(39) Kong, X.; Shan, M.; Terskikh, V.; Hung, I.; Gan, Z.; Wu, G. Solid-State ^{17}O NMR of Pharmaceutical Compounds: Salicylic Acid and Aspirin. *J. Phys. Chem. B* **2013**, *117*, 9643−9654.
(40) Vogt, F. G.; Yin, H.; Forcino, R. G.; Wu, L. ^{17}O Solid-State NMR as a Sensitive Probe of Hydrogen Bonding in Crystalline and Amorphous Solid Forms of Diflunisal. *Mol. Pharmaceutics* **2013**, *10*, 3433−3446.
(41) Kong, X.; Terskikh, V.; Toubaei, A.; Wu, G. A solid-state ^{17}O NMR study of platinum-carboxylate complexes: carboplatin and oxaliplatin. *Can. J. Chem.* **2015**, *93*, 945−953.
(42) Thurber, K. R.; Tycko, R. Measurement of sample temperatures under magic-angle spinning from the chemical shift and spin-lattice relaxation rate of ^{79}Br in KBr powder. *J. Magn. Reson.* **2009**, *196*, 84−87.
(43) Taylor, R. E. ^{13}C CP/MAS: Application to glycine. *Concepts Magn. Reson.* **2004**, *22A*, 79−89.
(44) Harris, R. K.; Becker, E. D.; Cabral De Menezes, S. M.; Granger, P.; Hoffman, R. E.; Zilm, K. W. Further conventions for NMR shielding and chemical shifts. *Pure Appl. Chem.* **2008**, *80*, 59−84.
(45) Massiot, D.; Fayon, F.; Capron, M.; King, I.; Le Calve, S.; Alonso, B.; Durand, J.-O.; Bujoli, B.; Gan, Z.; Hoatson, G. Modeling one- and two-dimensional solid-state NMR spectra. *Magn. Reson. Chem.* **2002**, *40*, 70−76.
(46) Clark, S. J.; Segall, M. D.; Pickard, C. J.; Hasnip, P. J.; Probert, M. I. J.; Refson, K.; Payne, M. C. First principles methods using CASTEP. *Z. Kristallogr. - Cryst. Mater.* **2005**, *220*, 567−570.
(47) Perdew, J. P.; Burke, K.; Ernzerhof, M. Generalized Gradient Approximation Made Simple. *Phys. Rev. Lett.* **1996**, *77*, 3865−3868.
(48) Pickard, C. J.; Mauri, F. All-electron magnetic response with pseudopotentials: NMR chemical shifts. *Phys. Rev. B: Condens. Matter Mater. Phys.* **2001**, *63*, 245101/1−245101/13.
(49) Yates, J. R.; Pickard, C. J.; Mauri, F. Calculation of NMR chemical shifts for extended systems using ultrasoft pseudopotentials. *Phys. Rev. B: Condens. Matter Mater. Phys.* **2007**, *76*, 024401/1−024401/11.
(50) Hammer, B.; Hansen, L. B.; Nørskov, J. K. Improved adsorption energetics within density-functional theory using revised Perdew-Burke-Ernzerhof functionals. *Phys. Rev. B: Condens. Matter Mater. Phys.* **1999**, *59*, 7413−7421.
(51) Grimme, S. Semiempirical GGA-type density functional constructed with a long-range dispersion correction. *J. Comput. Chem.* **2006**, *27*, 1787−1799.
(52) Holmes, S. T.; Iuliucci, R. J.; Mueller, K. T.; Dybowski, C. Semi-empirical refinements of crystal structures using ^{17}O quadrupolar-coupling tensors. *J. Chem. Phys.* **2017**, *146*, 064201.
(53) Holmes, S. T.; Engl, O. G.; Srnec, M. N.; Madura, J. D.; Quiñones, R.; Harper, J. K.; Schurko, R. W.; Iuliucci, R. J. Chemical Shift Tensors of Cimetidine Form A Modeled with Density

https://dx.doi.org/10.1021/acs.cgd.0c01164
Cryst. Growth Des. 2020, 20, 7484−7491

Functional Theory Calculations: Implications for NMR Crystallography. *J. Phys. Chem. A* **2020**, *124*, 3109−3119.
(54) Gilli, G.; Bellucci, F.; Ferretti, V.; Bertolasi, V. Evidence for resonance-assisted hydrogen bonding from crystal-structure correlations on the enol form of the β-diketone fragment. *J. Am. Chem. Soc.* **1989**, *111*, 1023−8.
(55) Berglund, B.; Vaughan, R. W. Correlations between proton chemical shift tensors, deuterium quadrupole couplings, and bond distances for hydrogen bonds in solids. *J. Chem. Phys.* **1980**, *73*, 2037−43.
(56) Jeffrey, G. A.; Yeon, Y. The correlation between hydrogen-bond lengths and proton chemical shifts in crystals. *Acta Crystallogr., Sect. B: Struct. Sci.* **1986**, *B42*, 410−13.
(57) Kaliaperumal, R.; Sears, R. E. J.; Ni, Q. W.; Furst, J. E. Proton chemical shifts in some hydrogen-bonded solids and a correlation with bond lengths. *J. Chem. Phys.* **1989**, *91*, 7387−91.
(58) Wu, G.; Freure, C. J.; Verdurand, E. Proton chemical shift tensors and hydrogen bond geometry: A ^{1}H-^{2}H dipolar NMR study of the water molecule in crystalline hydrates. *J. Am. Chem. Soc.* **1998**, *120*, 13187−13193.
(59) Brunner, E.; Sternberg, U. Solid-state NMR investigations on the nature of hydrogen bonds. *Prog. Nucl. Magn. Reson. Spectrosc.* **1998**, *32*, 21−57.
(60) Hibbert, F.; Emsley, J. Hydrogen bonding and chemical reactivity. *Adv. Phys. Org. Chem.* **1990**, *26*, 255−79.
(61) Cleland, W. W. Low-barrier hydrogen bonds and low fractionation factor bases in enzymic reactions. *Biochemistry* **1992**, *31*, 317−19.
(62) Cleland, W. W.; Kreevoy, M. M. Low-barrier hydrogen bonds and enzymic catalysis. *Science* **1994**, *264*, 1887−90.
(63) Guthrie, J. P. Short strong hydrogen bonds: can they explain enzymic catalysis? *Chem. Biol.* **1996**, *3*, 163−170.
(64) Shan, S.-O.; Herschlag, D. The change in hydrogen bond strength accompanying charge rearrangement: implications for enzymic catalysis. *Proc. Natl. Acad. Sci. U. S. A.* **1996**, *93*, 14474−14479.
(65) Warshel, A.; Papazyan, A. Energy considerations show that low-barrier hydrogen bonds to not offer a catalytic advantage over ordinary hydrogen bonds. *Proc. Natl. Acad. Sci. U. S. A.* **1996**, *93*, 13665−13670.
(66) Gerlt, J. A.; Kreevoy, M. M.; Cleland, W. W.; Frey, P. A. Understanding enzymic catalysis: the importance of short, strong hydrogen bonds. *Chem. Biol.* **1997**, *4*, 259−267.
(67) Tuckerman, M. E.; Marx, D.; Klein, M. L.; Parrinello, M. On the quantum nature of the shared proton in hydrogen bonds. *Science* **1997**, *275*, 817−820.
(68) Cleland, W. W.; Frey, P. A.; Gerlt, J. A. The low barrier hydrogen bond in enzymic catalysis. *J. Biol. Chem.* **1998**, *273*, 25529−25532.
(69) Kumar, G. A.; McAllister, M. A. Characterization of Low-Barrier Hydrogen Bonds. 8. Substituent Effects on the Strength and Geometry of the Formic Acid-Formate Anion Model System. An ab Initio and DFT Investigation. *J. Am. Chem. Soc.* **1998**, *120*, 3159−3165.
(70) Perrin, C. L. Are Short, Low-Barrier Hydrogen Bonds Unusually Strong? *Acc. Chem. Res.* **2010**, *43*, 1550−1557.
(71) Lu, J.; Hung, I.; Brinkmann, A.; Gan, Z.; Kong, X.; Wu, G. Solid-state ^{17}O NMR reveals hydrogen-bonding energetics: Not all low-barrier hydrogen bonds are strong. *Angew. Chem., Int. Ed.* **2017**, *56*, 6166−6170.
(72) Dračínský, M.; Vícha, J.; Bártová, K.; Hodgkinson, P. Towards accurate predictions of proton NMR parameters in molecular solids. *ChemPhysChem* **2020**, *21*, 2075−2083.

https://dx.doi.org/10.1021/acs.cgd.0c01164
Cryst. Growth Des. 2020, 20, 7484−7491